Shear-Induced Order in Aqueous Micellar Solutions of Amphiphilic Poly(*tert*-butylstyrene)-*b*-poly(Na methacrylate) Diblock

Bernard Leyh,*,†,⊥ Serge Creutz,‡ Jean-Pierre Gaspard,§ Claudie Bourgaux,|| and Robert Jérôme‡

Laboratoire de Dynamique Moléculaire, Institut de Chimie, B6c, Centre d'Etude et de Recherche sur les Macromolécules (CERM) B6a, and Laboratoire de Physique de la Matière Condensée, Institut de Physique, B5, Université de Liège, 4000 Sart-Tilman, Belgium, and LURE, Université de Paris-Sud, Bâtiment 209D, F. 91405 Orsay Cedex, France

Received June 9, 1998; Revised Manuscript Received October 1, 1998

ABSTRACT: Shear-induced order of aqueous micellar solutions of a poly(*tert*-butylstyrene)-*b*-poly(sodium methacrylate) diblock ($c = 2.5-15$ w/v %) has been investigated by small-angle X-ray scattering. Data collected from a Couette cell in both radial and tangential geometries agree with a crystalline ordering of micelles in close packed hexagonal layers perpendicular to the velocity gradient, when c is in the 5−10 w/v % range. The measured interlayer distance is indeed very close to the value expected for a close-packed structure. The experimental data are consistent with a zigzag motion of adjacent planes upon shear. Shear-induced order is, however, restricted to a narrow concentration range just above the concentration for the sol−gel transition. This domain is thought to correspond to a regime where relative layer translation modes are allowed whereas mutual rotation is hindered.

1. Introduction

The immiscibility of the constitutive polymeric components of block copolymers accounts for the strong tendency of these materials to self-associate with formation of a variety of usually well organized microstructures. This behavior may be observed either in the melt[1] or in solution in a selective solvent of one of the blocks at concentrations higher than the critical micellar concentration. The characteristic size of these organized systems ranges from a few nanometers to hundreds of nanometers. Application of appropriate external electrical fields, for example in the kilovolt per centimeter range, is a way to impart preferential orientation over a macroscopic scale to the microdomains formed by some block copolymers, in thin films.[2] Another powerful strategy, directly related to this work, consists of shearing block copolymers. For instance, it has been shown[3−5] that lamellae of a diblock copolymer could be preferentially oriented with respect to the velocity gradient vector, simply by tuning the frequency of an oscillatory shearing deformation.

The pioneering works by Hoffman[6] and Ackerson and Clark[7] have initiated an intense activity in the field of shear-induced transitions in colloidal systems. Crystallization of colloidal suspensions of both inorganic and polymer spheres has been studied by various authors.[8−13] Fcc or bcc organizations have been frequently observed, but evidence for a hcp stacking sequence emerged from the recent work of Clarke et al.[8] In the case of block copolymer micelles, most of the experimental work has focused on a limited number of systems, mainly in organic solvents but also in water, using small angle scattering of either neutrons (SANS) or X-rays (SAXS). Neutral diblock copolymers of polystyrene-*b*-poly(ethylene-*co*-propylene) in dodecane at 3 wt % showed diffraction patterns characteristic of long-range order at low shear rates.[14] McConnell et al.[15,16] investigated diblocks of polystyrene-*b*-polyisoprene in decane in the 12−85 wt % range. Depending on the block sizes, bcc or fcc structures were observed. Hamley et al.[17] determined the concentration−temperature phase diagram for di- and triblock copolymers of polystyrene and polyisoprene dissolved in di-*n*-butyl phthalate (polymer volume fractions in the 0.1−0.4 range) and observed transitions from an hexagonal to a lamellar ordered structure upon increasing concentration. Phase transitions between fcc, bcc and hexagonally packed rod structures are related to both the concentration and temperature, as observed in the work by Pople et al.[18] on poly(ethylene oxide)-*b*-poly(butylene oxide) in a 0.2 mol/L aqueous K_2SO_4 solution ($c = 23-38$ wt %). Kleppinger et al.[19,20] followed the response to shear of solutions of polystyrene-*b*-poly(ethylene-*co*-butylene)-*b*-polystyrene triblocks in a non polar organic solvent ($c = 20-40$ wt %) by using both SAXS and SANS. This study led them to infer the appearance of a single crystalline phase of twinned bcc structure. Diat et al.,[21] Berret et al.,[22,23] and Mortensen[24] also observed cubic structures in aqueous solutions of triblock copolymers based on poly(ethylene oxide) and poly(propylene oxide) submitted to shear. The concentration ranges covered in these works were different, i.e., <5 wt % to 40% in ref 21, 20−35 wt % in ref 23, and 55 wt % in ref 24. The temperature dependence of the micellar structure observed by shearing aqueous solutions of poly(ethylene oxide)-*b*-poly(propylene oxide)-*b*-poly(ethylene oxide) triblocks was studied by King et al.[25] Other triblocks, for instance poly(ethylene oxide)-*b*-poly(isobutylene oxide)-*b*-poly(ethylene oxide) ($c = 1-30$ wt %; $T = 7-70$ °C)[26] also showed an ordering behavior under shear flow. Shear stress often results in long-range order within layers parallel to the velocity vector. These layers stack in the direction of the velocity gradient. In contradiction to these experimental observations, molecular dynamics

† Institut de Chimie, B6c, Universitéde Liège.
‡ Centre d'Etude et de Recherche sur les Macromolécules (CERM), Université de Liège.
§ Institut de Physique, B5, Université de Liège.
|| Université de Paris-Sud.
⊥ Chercheur qualifié du FNRS (Belgium).

10.1021/ma980918z CCC: $15.00
Published on Web 12/08/1998

simulations[27,28] predict an ordered phase in the plane perpendicular to the flow, under a relatively high shear rate, however.

In this work, aqueous solutions of an amphiphilic diblock copolymer that combines a hydrophobic poly(*tert*-butylstyrene) block ($\bar{M}_n = 2900$) and a hydrophilic Na polymethacrylate one ($\bar{M}_n = 7400$) are deformed at constant shear rates spanning from $\dot{\gamma} = 0$ to 570 s^{-1}, in a Couette cell. The experimental data are collected at room temperature for solution concentrations of 2.5, 5.0, 7.5, 10, and 15 w/v %. This concentration range brackets the sol−gel transition of this system, which has been found to take place close to 3.5 w/v %. The purpose is to analyze in detail the crystalline order promoted by these specific conditions and the type of sliding motion taking place in the shear field. This is, to our knowledge, the first example of a shear induced long-range crystallized phase in aqueous solution of a polyelectrolyte containing block copolymer. Furthermore, SAXS data are collected in both the radial and tangential geometries so that a picture of the three-dimensional reciprocal space can emerge. Information about the lattice parameter for the ordered planes, the interplanar distance, and the stacking sequence is extractable from these experimental data.

2. Experimental Section

2.1 Copolymer Synthesis. The poly(*tert*-butylstyrene)-*b*-sodium polymethacrylate copolymer was synthesized as follows. *tert*-butylstyrene (tBS), α-methylstyrene (αMeS), and *tert*-butyl methacrylate (tBMA) were first vacuum distilled from calcium hydride and then stored under a nitrogen atmosphere at −20 °C. Before polymerization, all monomers were diluted with an equal volume of toluene. Triethylaluminum (1 M in toluene) was added to tBMA until a yellowish green color was observed. Fluorenyllithium was dropwise added to tBS and αMeS, respectively, until a persistent orange color was observed. The monomers were recovered by distillation under reduced pressure. 1,1-Diphenylethylene was dried and redistilled over *sec*-butyllithium just before polymerization.

Lithium chloride was flame-dried under vacuum just prior to polymerization and stored under nitrogen. THF was purified by reflux over a freshly prepared sodium−benzophenone complex.

Polymerization was carried out under dry nitrogen in flasks equipped with three-way stopcocks capped with rubber septa. All glassware was flamed under vacuum before use. Solutions were transferred via stainless steel capillaries or with glass syringes through the septa.

After the reactor was loaded with a 10-fold molar excess of LiCl with respect to the initiator, THF and a few drops of αMeS were added. The solution was cooled to −78 °C and dropwise titrated with *sec*-butyllithium until a persistent orange/red color was observed. The required amount of the initiator was added to the polymerization medium, followed by tBS, whereupon the polymerization was performed for 30 min. Poly(*tert*-butylstyrene) chains were end-capped with 1,1-diphenylethylene and an aliquot was withdrawn for characterization, followed by tBMA addition. The final copolymer concentration was 50 g/L. The copolymerization reaction was quenched with degassed methanol after 2 h. The copolymer was recovered by precipitation in water and the comonomer conversion was close to completion.

2.2 Copolymer Characterization. Size exclusion chromatography (SEC) was carried out in THF at 35 °C, using a Hewlett-Packard 1050 liquid chromatograph equipped with four PLGel Columns (100, 500, 1000, and 10000 Å) and a Hewlett-Packard 1047A refractive index detector. Polystyrene standards were used for calibration. The copolymer composition was analyzed before hydrolysis by ^{1}H NMR with a Brüker AN 400 superconducting magnet spectrometer.

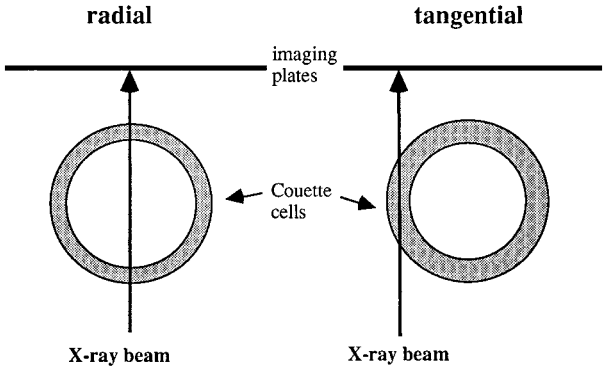

Figure 1. Radial and tangential geometries for the SAXS experiments with a Couette cell. In the radial experiment, the incident beam is parallel to the velocity gradient ($\vec{\nabla}v$). In the tangential configuration, the incident beam is parallel to the velocity ($\vec{v}$).

2.3 Hydrolysis. The tBMA block was hydrolyzed by refluxing the copolymer overnight in a 5/1 v/v dioxane/37% HCl solution. The hydrolyzed copolymer was recovered by solvent distillation under vacuum and redissolution in aqueous NaOH or CsOH. Finally, the copolymer was purified by dialysis against demineralized water.

2.4 SAXS. X-ray scattering experiments were conducted at the D24 beamline of the LURE-DCI synchrotron radiation source (Orsay, France). The scattering patterns were recorded at $\lambda = 1.49$ Å with imaging plates. A Couette cell was designed to carry out in situ X-ray studies of complex fluids under shear flow. It consists of two concentric cylinders (gap between cylinders 0.5 mm (radial geometry) or 1 mm (tangential geometry), outer radius 10 mm). The shear rate ranges from 0 to 570 s^{-1}. The X-ray path crosses either the center or the edge of the cell so that the beam is parallel either to the shear gradient $\vec{\nabla}v$ (radial geometry) or to the velocity $\vec{v}$ (tangential geometry) (Figure 1). The vorticity direction will be denoted as $\vec{e} = \vec{v} \wedge \vec{\nabla}v$. The sample−detector distance was equal to 200 cm or to 210.5 cm.

3. Experimental Results and Crystallographic Analysis

Figure 2 shows the diffraction spectra obtained in the radial geometry at very low shear rate ($\dot{\gamma} = 1$ s^{-1}) and at shear rates of 200 and 570 s^{-1} for a concentration of 5 w/v %. Whereas a pattern with circular diffraction rings is observed at very small shear rates (Figure 2a), diffraction spots characteristic of an ordering process start to appear already at $\dot{\gamma} = 5$ s^{-1}. This ordering improves upon increasing shear rate, as exemplified in Figure 2b ($\dot{\gamma} = 200$ s^{-1}) and 2c ($\dot{\gamma} = 570$ s^{-1}). The diffraction pattern shows an hexagonal symmetry and extends up to the eighth diffraction order. Figure 3 displays similar data at $c = 7.5$ w/v %.

At a concentration of 2.5 w/v %, no ordering takes place. At $c = 5$ or 7.5%, the ordered structure remains even at the highest shear rate available (570 s^{-1}), whereas at 10%, the ordering is observed around $\dot{\gamma} =$ 20 s^{-1} but disappears at shear rates larger than 50 s^{-1}. At a concentration of 15%, the diffraction pattern remains isotropic in the whole shear rate range investigated, so that we can conclude that the long-range ordering of these micellar solutions is limited to a relatively narrow concentration range, viz. 5−10 w/v %. Experiments have also been conducted with a poly(*tert*-butylstyrene)-*b*-poly(cesium methacrylate) copolymer, but in that case, no crystalline order appears under shear.

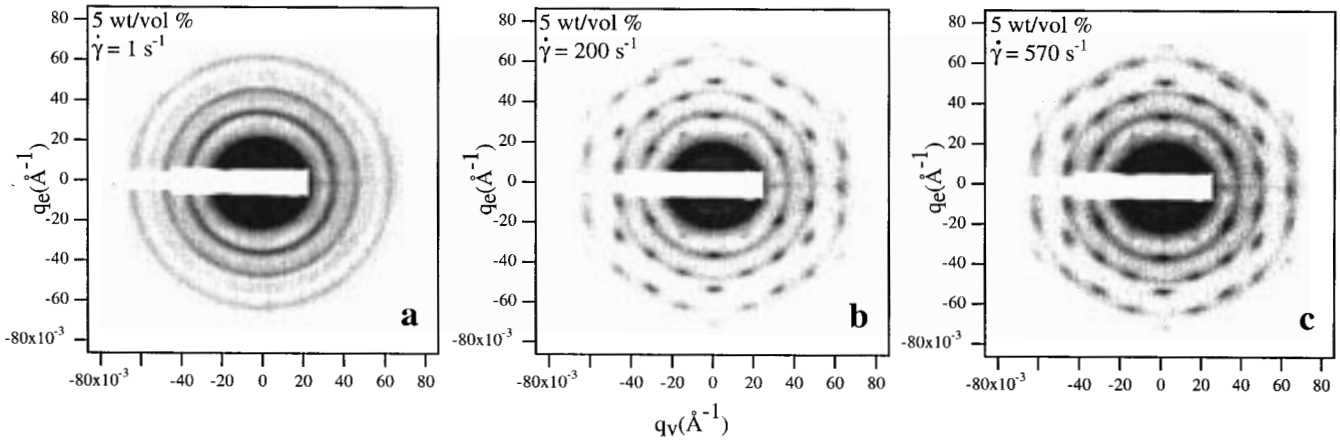

Figure 2. Diffraction patterns obtained in the radial configuration for poly(*tert*-butylstyrene)(19)-*b*-poly(sodium methacrylate)(70) (c = 5 w/v % in H_2O): (a) $\dot{\gamma}$ = 1 s^{-1}; (b) $\dot{\gamma}$ = 200 s^{-1}; (c) $\dot{\gamma}$ = 570 s^{-1}.

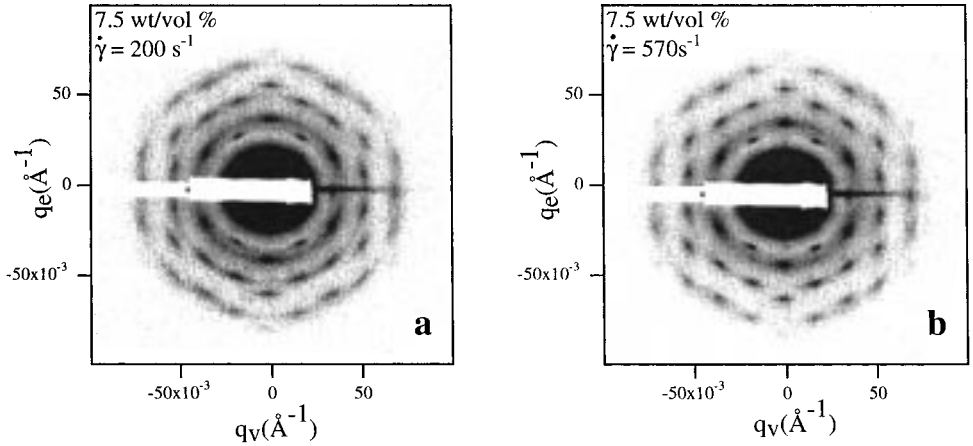

Figure 3. Diffraction patterns obtained in the radial configuration for poly(*tert*-butylstyrene)(19)-*b*-poly(sodium methacrylate)(70) (c = 7.5 w/v % in H_2O): (a) $\dot{\gamma}$ = 200 s^{-1}; (b) $\dot{\gamma}$ = 570 s^{-1}.

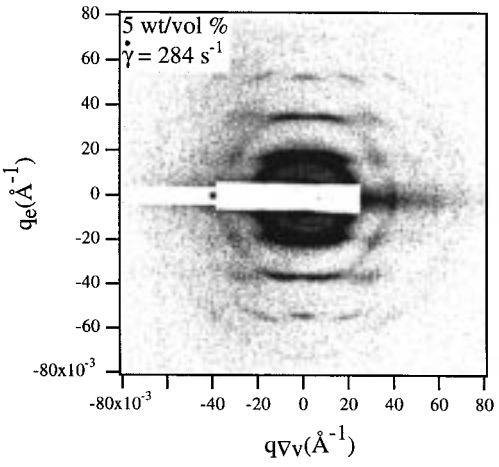

Figure 4. Diffraction patterns obtained in the tangential configuration for poly(*tert*-butylstyrene)(19)-*b*-poly(sodium methacrylate)(70) (c = 5 w/v % in H_2O) with $\dot{\gamma}$ = 284 s^{-1}.

The data obtained in tangential geometry show a few diffraction rods parallel to the shear gradient direction (Figure 4). In addition, these rods display an intensity modulation from which information on the layer stacking can be inferred.

The diffraction rings obtained at rest or sufficiently low shear rate (Figure 2a) are compatible with a polycrystalline system of face-centered cubic structure characterized by an intermicellar distance equal to, respectively, 426 ± 4 Å (c = 5%), 384 ± 4 Å (c = 7.5%), 339 ± 4 Å (c = 10%) and 305 ± 4 Å (c = 15%). This intermicellar distance, a, is found to be proportional to a power of the concentration, viz. $a \propto c^{\beta}$ with $\beta = -0.34 \pm 0.02$, and thus very close to the inverse of the cubic root of the copolymer concentration. Such a behavior is indicative of repulsive interactions. An average micellar aggregation number of 155 ± 10 has been estimated from the comparison of the copolymer concentration and of the micellar concentration. This latter concentration is directly related to the above-mentioned intermicellar distance. At those concentrations, gelation takes place. An estimate of the Debye screening length at lower concentration, e.g. 1 w/v %, leads to a value of about 30 Å, if we assume a free charge fraction close to 0.3 for the methacrylate chains, as has been proposed in the case of sodium polyacrylate[29−31] and in the case of sodium polymethacrylate.[32] It is interesting to notice that analogies have been found in the ionization dynamics of sodium and lithium polyacrylate chains, on one side, and of poly(methyl methacrylate)-*b*-poly(Na or Li acrylate) micellar solutions, on the other side.[33] Note that no salt has been added to our copolymer solutions. In a previous work,[34] the external radius for these micelles has been found to be equal to 200 Å, so that a repulsive behavior is indeed expected at the intermicellar distances corresponding to the concentrations investigated in this paper.

In the absence of shear-induced long range ordering, at c = 5 w/v %, a correlation length of 2300 ± 300 Å was inferred from the width at half-height of the first

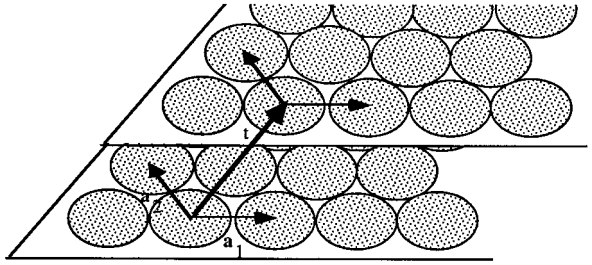

Figure 5. Definition of the basis vectors for the micellar planes and of the translation vector connecting the basis planes.

scattering peaks. At c = 10 w/v %, the correlation length amounts to 1900 ± 500 Å. In both cases, it is equal to 5−6 times the intermicellar distance, whereas for a liquid the correlation length is not expected to exceed two or three interparticle distances. We thus excluded a liquid structure in favor of a randomly oriented polycrystal, which is then the starting point for the experiments in a shear field.

When crystalline ordering takes place, our diffraction data can be interpreted on the basis of the formalism explained hereafter. The diffracted amplitude $A(\vec{q})$ is the Fourier transform of the density of diffracting objects:

$$A(\vec{q}) = A_0(q)\sum_j e^{-i\vec{q}\cdot\vec{r}_j} \quad (1)$$

$A_0(q)$ is a factor characteristic of the individual micelles, which is a function of the modulus of $\vec{q}$. Its square gives the form factor, $P(q)$. $\vec{r}_j$ is the position vector of the center of the jth micelle. For spherical identical micelles, $A_0(q)$ factorizes out in all equations and will therefore be no longer considered in this paper, although it must be kept in mind that this factor leads to a slightly modulated intensity decrease as q increases. As the radius of the Ewald sphere is large compared to the modulus of the scattering vector under small angle conditions, this sphere can be replaced by its tangent plane, providing us directly with $(\vec{v}, \vec{e})$ and $(\vec{\nabla}v, \vec{e})$ planar cross sections of the reciprocal space, using the radial and tangential geometries, respectively. The data of Figures 2−4 strongly suggest the occurrence of maximum density layers parallel to the velocity vector. Taking vectors $\vec{a}_1$ and $\vec{a}_2$ as basis vectors within these planes (Figure 5), the scattering amplitude is then equal to

$$A(\vec{q}) = \Big(\sum_{\substack{\text{integer}\\ m,n}} e^{-i\vec{q}\cdot(m\vec{a}_1+n\vec{a}_2)}\Big)\sum_p e^{-i\vec{q}\cdot\vec{t}_p} = \Pi(\vec{q})\cdot L(\vec{q}) \quad (2)$$

$\vec{t}_p$ corresponds to the translation vector connecting the different basis planes.

Our analysis is based on this factorization in which the first factor, $\Pi(\vec{q})$, characterizes the order within the layers and the second one, $L(\vec{q})$, describes the correlation between the layers. The reciprocal lattice for a single dense plane consists of parallel "tubes" organized in an hexagonal configuration.[23,35] Different types of layer stacking can take place leading either to an hexagonal close packed structure or to a face-centered cubic structure or to a random stacking structure (also called highly twinned fcc). These different structures give rise to different modulations of the $L(\vec{q})$ factor[35] which allows them to be discriminated.

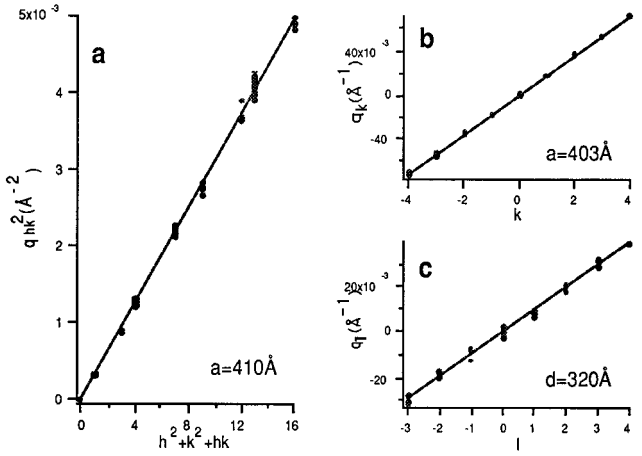

Figure 6. Analysis of the diffraction data of Figures 2 and 4: (a) Radial geometry (eq 4); (b) tangential geometry with tube locations along the $\vec{q}_e$ direction (eq 5); (c) tangential geometry with tube modulation along the $\vec{q}_{\nabla v}$ direction (eq 6).

The Bragg peak positions for a hexagonal layer are given by

$$\vec{q}_{hk} = h\vec{a}_1^* + k\vec{a}_2^* \quad (3)$$

where $\vec{a}_1^*$ and $\vec{a}_2^*$ are the reciprocal space basis vectors. We take $\vec{a}_2^*$ parallel to the vorticity direction $\vec{e}$. This leads to

$$q_{hk}^2 = \left(\frac{4\pi}{\sqrt{3}a}\right)^2(h^2 + k^2 + hk) \quad (4)$$

It can easily be shown that the reflections corresponding to $h^2 + k^2 + hk = 1$ are forbidden for a fcc-stacking of (111) planes. On the other hand, for a hcp-stacking of (0001) planes, as well as for a random stacking, these reflections are allowed.[35] The data of Figures 2 and 3 show that the q^2 ratio betwen the first two rings is equal to 3, thus excluding the fcc-stacking of (111) planes. The analysis of the radial diffraction data using eq 4. leads to lattice parameters of 410 ± 7 Å (c = 5 w/v %), 370 ± 5 Å (c = 7.5 w/v %) and 345 ± 5 Å (c = 10 w/v %). Figure 6a illustrates the data analysis in the 5% case. Increasing the shear rate from 200 to 570 s^{-1} does not lead to structural changes, within experimental errors. Lattice parameter changes smaller than 5 Å were deduced.

The spacing between the tubes in the tangential spectra gives also directly the lattice parameter of the dense planes in direct space, according to

$$q_k = \frac{\vec{q}_{0kl}\cdot\vec{a}_2^*}{|\vec{a}_2^*|} = \frac{4\pi}{\sqrt{3}a}k \quad (5)$$

At c = 5 w/v %, this leads to a = 403 ± 2 Å, in good agreement with the radial geometry data (Figure 6b). This value has to be compared with the external micellar radius obtained in the Guinier regime in dilute solutions: R = 200 Å.[34] According to Loose and Ackerson,[35] for the hcp and random stacking structures, the modulation of the tubes corresponding to k = 1 (inner ring) and k = 2 (third ring) gives rise to maxima at

$$q_l = \frac{\vec{q}_{0kl}\cdot\vec{a}_3^*}{|\vec{a}_3^*|} = l\frac{\pi}{d} \quad (6)$$

where l is odd, $\vec{a}_3^*$ is parallel to the velocity gradient, and d is the interplanar spacing. On the other hand, for $k = 3$ (fifth ring), peak positions are given by eq 6. with even l values. From the data of Figure 4, an interplanar spacing of 320 ± 10 Å is calculated for $c =$ 5 w/v % (Figure 6c). The d/a ratio, equal to 0.80 ± 0.04, is very close to the $(2/3)^{1/2}$ ratio characteristic of close packing.

The stacking can be characterized by a parameter which we will call α (and which corresponds to parameter "*a*" of Loose and Ackerson[35]). To define this parameter, we have to consider the three different possible types of registered sites of a hexagonal layer, called A, B, and C. If the stacking of hexagonal layers corresponds to an ABABAB... sequence, then a hcp structure is formed, whereas a fcc crystal results from an ABCABCABC... stacking. α is defined as the probability that two successive stacking operations are described by the same translation vector t_p. If α is equal to 1, then we have a perfect ABCABC stacking sequence and thus a fcc structure. At the opposite, $\alpha = 0$ defines a perfect hcp organization. For a random stacking of hexagonal dense planes, α is equal to 0.5. For the tubes corresponding to the inner diffraction ring, we have fitted the diffracted intensity vs q_l to eq 8 of Loose and Ackerson[35] and deduced $\alpha = 0.51 \pm 0.01$ at $c = 5$ w/v %, indicating clearly a random stacking organization, which is equivalent to a highly twinned fcc structure.

Up to now, our analysis focused on extracting structural information from diffraction peak positions. We are, however, in a dynamical situation, where the shear modifies the intensity ratios with respect to the static situation. Loose and Ackerson[35] also derived formula for the shear-induced intensity modulations in the ($\vec{v}$, $\vec{e}$) plane (radial geometry) and in the ($\vec{\nabla}v$, $\vec{e}$) plane (tangential geometry). They considered two limiting sliding cases: the so-called zigzag motion with respect to a reference plane, which corresponds to successive jumps between given positions, registered or not, of the close-packed lattice, and the sliding plane motion, where the micelles follow straight paths along the velocity direction. In this second case, the (0,1) and $(0,\bar{1})$ peaks of the inner ring become forbidden, in disagreement with our data (Figures 2 and 3), thus excluding this type of motion.

Compared to the static random stacking (highly twinned fcc) in which the peaks of a given diffraction ring all have the same intensity, for symmetry reasons, the zigzag motion introduces intensity modulations within such a given diffraction ring. Our experimental data show a slight modulation, qualitatively similar to Figure 5b in the paper of Loose and Ackerson.[35] To take this aspect into account, these authors[35] introduced new translation vectors $\vec{r}_1$ and $\vec{r}_2$, which replace the usual translation vectors connecting the A, B, and C registered sites of close-packed structures. These new vectors are defined by eq 7, where $\vec{v}_o$, $(\vec{\nabla}v)_o$, and $\vec{e}_o$ are unitary

$$\vec{r}_1 = a\left(C\vec{v}_o + \sqrt{\frac{2}{3}}(\vec{\nabla}v)_o + \frac{1-C}{\sqrt{3}}\vec{e}_o\right)$$

$$\vec{r}_2 = a\left(C\vec{v}_o + \sqrt{\frac{2}{3}}(\vec{\nabla}v)_o - \frac{1-C}{\sqrt{3}}\vec{e}_o\right) \qquad (7)$$

vectors. As we consider that the X photons "see" an instantaneous situation, the C parameter is fixed. It can take values in the 0−0.5 range. $C = 0.5$ corresponds to the usual translation vectors for close-packed crystals. In the presence of shear induced long-range ordering, all our data are very similar, whatever the concentration or the shear rate. In the first ring, the (0,1) and $(0,\bar{1})$ peaks are less intense by a factor 1.05 ± 0.04 than the other ones. At the opposite, in the third ring, the (0,2) and $(0,\bar{2})$ peaks are about 1.3 ± 0.1 time larger than the other ones. From these values, we can estimate that $C = 0.494 \pm 0.004$. This is thus in favor of a zigzag motion during which the micelles spend most of their time in registered sites (A, B or C). We did not observe any decrease of the C parameter upon shear rate increase, indicating that we remained within a slow shear regime. This regime has been coined "slip−stop−slip motion" by McConnell et al.,[15] who observed it at slow shear rate.

4. Discussion

From the data presented in section 3, the following picture emerges. In a shear field, the initially polycrystalline micellar solution orders in dense hexagonal planes which stack along the velocity gradient. The motion of the individual planes can be thought as successive jumps between registered sites. This behavior is, however, limited to a relatively narrow concentration range (5−10 w/v %). Furthermore, in all the cases where we could observe this long-range crystalline ordering, the transition from the disordered phase to the ordered phase occurred at a concentration just above the concentration for the sol−gel transition. The unsuccessful experiments with poly(*tert*-butylstyrene)-*b*-poly(cesium methacrylate) indicate also the important role of the counterion. In the case of classical anionic surfactants, cesium tends to be more tightly bound to the micellar aggregate than sodium.[36,37] As a consequence, the ionic character of the surfactant is altered and a denser packing is then observed due to the reduction of the electrostatic repulsion. The same phenomenon is expected to hold true for polymeric surfactants. The absence of ordering would then emanate from the higher counterion binding, which depresses the long-range electrostatic repulsion between micelles.

We suggest a simple mechanical model to explain qualitatively the observed behavior of these micellar solutions. Below the sol−gel transition concentration, the micellar solution appears as a liquid with a standard interference function showing three peaks. No long range order appears upon shearing, as is also the case far above the sol−gel transition concentration. In the latter situation, the shear presumably produces internal fractures and the velocity gradient is nonconstant. In the gel phase, just above the sol−gel transition, the response to the shear is interpreted as follows. In response to the planar shear, micelles order in planes perpendicular to $\vec{\nabla}v$. The planes have to be as dense as possible in order to maximize the interplanar distances and to favor the glide. As we are in a concentration range where the micelles percolate, an easy glide is obtained when the micelles are ordered on the nodes of a triangular lattice identical to the (111) dense planes of a fcc lattice or the (0001) planes of an hexagonal lattice. Assuming rigid dense planes, it is easy to figure out that there are two potential energy barriers of different heights. The lower barrier corresponds to a translation along the $^2/_3\vec{a}_1 + {}^1/_3\vec{a}_2 = a({}^1/_2\vec{v}_o + ({}^1/_{2\sqrt{3}})\vec{e}_o)$ (or equivalent) direction and a higher barrier corre-

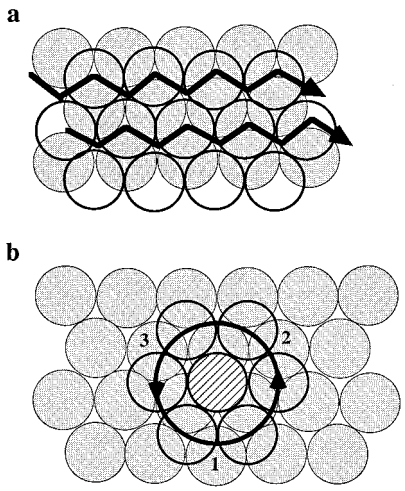

Figure 7. Types of interplane motion which can take place in a shear field: (a) zigzag translation along the $^2/_3\vec{a}_1 + {}^1/_3\vec{a}_2$ and $^1/_3\vec{a}_1 - {}^1/_3\vec{a}_2$ directions, where the glide motion is indicated by the heavy line; (b) rotation of the upper plane with respect to the lower (shaded) plane around the hatched micelle. The motion of the micellar centers is indicated by the heavy circle. Potential energy maxima correspond to positions 1, 2, and 3, where some micelles are nearly superimposed on each another.

sponds to rotation (Figure 7). In a hard sphere limit, a packing fraction (ratio of the occupied volume to the total volume) $\eta = 2\pi/9 \approx 0.698 = \eta_{fcc}/1.061$ allows a free translation while the rotation is forbidden. For a free rotation, $\eta = \pi/3\sqrt{3} \approx 0.605 = \eta_{fcc}/1.225$, and in that range, no driving force is still present. It may therefore be expected that crystallization upon shear appears in a restricted concentration range.

A limited number of computer simulation experiments using non equilibrium molecular dynamics techniques have been performed.[27,28] The results do not coincide with our experimental findings but they at least show a similar tendency toward ordering. The main result of the simulation is the sudden drop of the diffusion coefficient in directions perpendicular to the flow at a given critical shear rate. The micellar displacements then become restricted in the shear plane. More computer simulation work on this system is required to better understand the mechanism of crystalline ordering.

Relaxation times associated with micellar diffusion, on one hand, and with polymer chain dynamics, on the other hand, have been shown to control the type of organization observed in shearing experiments.[4] In our experimental setup, the shear rate is small compared to the frequencies associated with both of these motions, so that they are averaged out. An interesting analogy may be noticed. In the low shear frequency regime, polystyrene-*b*-polyisoprene copolymer lamellae were found to orient parallel to the $(\vec{v}, \vec{e})$ plane, exactly as in our case, whereas, at higher shear frequency, the lamellae orient parallel to the $(\vec{v}, \vec{\nabla}v)$ plane. The latter orientation would correspond to the kind of organization evidenced in the above-mentioned simulation studies.[27,28]

In the particular case studied here, the long-range order remained even at the highest shear rate available (when $c = 5$ and 7.5 w/v %) or was stable only in a restricted shear rate range (when $c = 10$ w/v %). No systematic study has been performed on the evolution of the system after having stopped the shear. At 5 w/v %, it was observed that when one switches from the highest shear rate (570 s^{-1}) to rest, the diffraction pattern remained structured but blurred somewhat. However, the kinetics of the process has not been followed. Such effects clearly require further investigation. The influence of the temperature on this behavior needs to be investigated, too.

5. Conclusion

We have demonstrated the appearance of a monocrystalline-type order for diblock copolymer micelles of poly(*tert*-butylstyrene) and poly(sodium methacrylate) dissolved in water. SAXS measurements in a Couette cell in both the radial and tangential geometries lead to a three-dimensional sampling of the reciprocal space. Micelles are shown to organize in close-packed layers of hexagonal symmetry stacked along the velocity gradient. Our data are compatible with a random stacking of these planes, leading to a highly twinned fcc structure. This is coherent with previous observations of polymer colloid dispersions and non ionic diblock copolymers in both aqueous and organic solvants.[10,11,15,16,20−23,35] The ratio between the center-to-center intermicellar distance and the interlayer distance is found to be very close to that of a close-packed structure. The shear-induced motion of the individual dense planes is found to correspond to the zigzag model of Loose and Ackerson,[35] with jumps between positions extremely close to the registered sites. These data are thought to be characteristic of a concentration range where the packing allows for layer sliding via the zigzag motion but not for relative rotational motion of adjacent planes. Molecular dynamics simulation data would be very helpful to reach a deeper understanding of the long-range crystallization mechanism and of the different dynamic regimes which can be reached under low and higher shear rates.

Acknowledgment. We are grateful to Professor C. Houssier for an interesting discussion on polyelectrolyte solutions. S.C. and R.J. are grateful to the "Services Fédéraux des Affaires Scientifiques, Techniques et Culturelles" for general support to CERM in the frame of the "Pôles d'Attraction Interuniversitaires 4/11: Supramolecular Catalysis and Supramolecular Chemistry". Financial support from the "Commissariat Général aux Relations Internationales" (CGRI) and from the Belgian "Fonds National de la Recherche Scientifique" (FNRS) and Fonds de la Recherche Fondamentale Collective (FRFC) is gratefully acknowledged. S.C. and R.J. thank Akzo Nobel for financial support. B.L. thanks the Belgian FNRS for a research associate position.

References and Notes

(1) Bates, F. S.; Fredrickson, G. H. *Annu. Rev. Phys. Chem.* **1990**, *41*, 525−557.
(2) Morkved, T. L.; Lu, M.; Urbas, A. M.; Ehrichs, E. E.; Jaeger, H. M.; Mansky, P.; Russel, T. P. *Science* **1996**, *273*, 931−933.
(3) Koppi, K. A.; Tirrell, M.; Bates, F. S.; Almdal, K.; Colby, R. H. *J. Phys. II* **1992**, *2*, 1941−1959.
(4) Chen, Z.-R.; Kornfield, J. A.; Smith, S. D.; Grothaus, J. T.; Satkowski, M. M. *Science* **1997**, *277*, 1248−1253.
(5) Maring, D.; Wiesner, U. *Macromolecules* **1997**, *30*, 660−662.
(6) Hoffman, R. L. *Trans. Soc. Rheol.* **1972**, *16*, 155−173.
(7) Ackerson, B. J.; Clark, N. A. *Phys. Rev. Lett.* **1981**, *46*, 123−126.
(8) Clarke, S. M.; Rennie, A. R.; Ottewill, R. H. *Langmuir* **1997**, *13*, 1964−1969.
(9) Ackerson, B. J. *J. Phys.: Condens. Matter* **1990**, *2*, SA389−392.

(10) Ashdown, S.; Markovic, I.; Ottewill, R. H.; Lindner, P.; Oberthür, R. C.; Rennie, A. R. *Langmuir* **1990**, *6*, 303−307.
(11) Versmold, H.; Lindner, P. *Langmuir* **1994**, *10*, 3043−3045.
(12) Vos, W. L.; Megens, M.; Kats, C. M. v.; Bösecke, P. *Langmuir* **1997**, *13*, 6004−6008.
(13) Miguez, H.; Meseguer, F.; Lopez, C.; Mifsud, A.; Moya, J. S.; Vasquez, L. *Langmuir* **1997**, *13*, 6009−6011.
(14) Phoon, C. L.; Higgins, J. S.; Allegra, G.; Leeuwen, P. v.; Staples, E. *Proc. R. Soc. London A* **1993**, *442*, 221−230.
(15) McConnell, G. A.; Lin, M. Y.; Gast, A. P. *Macromolecules* **1995**, *28*, 6754−6764.
(16) McConnell, G. A.; Gast, A. P. *Macromolecules* **1997**, *30*, 435−444.
(17) Hamley, I. W.; Fairclough, J. P. A.; Ryan, A. J.; Ryu, C. Y.; Lodge, T. P.; Gleeson, A. J.; Pedersen, J. S. *Macromolecules* **1998**, *31*, 1188−1196.
(18) Pople, J. A.; Hamley, I. W.; Fairclough, J. P. A.; Ryan, A. J.; Komanschek, B. U.; Gleeson, A. J.; Yu, G.-E.; Booth, C. *Macromolecules* **1997**, *30*, 5721−5728.
(19) Kleppinger, R.; Reynders, K.; Mischenko, N.; Overbergh, N.; Koch, M. H. J.; Mortensen, K.; Reynaers, H. *Macromolecules* **1997**, *30*, 7008−7011.
(20) Kleppinger, R.; Mischenko, N.; Theunissen, E.; Reynaers, H. L.; Koch, M. H. J.; Almdal, K.; Mortensen, K. *Macromolecules* **1997**, *30*, 7012−7014.
(21) Diat, O.; Porte, G.; Berret, J.-F. *Phys. Rev. B* **1996**, *54*, 14869−14872.
(22) Berret, J.-F.; Molino, F.; Porte, G.; Diat, O.; Lindner, P. *J. Phys.: Condens. Matter* **1996**, *8*, 9513−9517.
(23) Berret, J.-F.; Molino, F. R.; Porte, G. *J. Phys. (Fr.)* **1998**, 0000.
(24) Mortensen, K. *Macromolecules* **1997**, *30*, 503−507.
(25) King, S. M.; Heenan, R. K.; Cloke, V. M.; Washington, C. *Macromolecules* **1997**, *30*, 6215−6222.
(26) Mortensen, K.; Talmon, Y.; Gao, B.; Kops, J. *Macromolecules* **1997**, *30*, 6764−6770.
(27) Erpenbeck, J. J. *Phys. Rev. Lett.* **1984**, *52*, 1333−1335.
(28) Xue, W.; Grest, G. S. *Phys. Rev. Lett.* **1990**, *64*, 419−422.
(29) Leyte, J. C.; Klink, J. J. v. d. *J. Chem. Phys.* **1975**, *62*, 749−750.
(30) Manning, G. S. *J. Chem. Phys.* **1975**, *62*, 748−749.
(31) Manning, G. S. *Q. Rev. Biophys.* **1978**, *11*, 179−246.
(32) Gustavsson, H.; Lindman, B.; Bull, T. *J. Am. Chem. Soc.* **1978**, *100*, 4655−4661.
(33) Kriz, J.; Masar, B.; Dybal, J.; Doskocilova, D. *Macromolecules* **1997**, *30*, 3302−3308.
(34) Gaspard, J.-P.; Creutz, S.; Bouchat, P.; Jérôme, R.; Cohen-Stuart, M. *Physica B* **1997**, *234−236*, 268−270.
(35) Loose, W.; Ackerson, B. J. *J. Chem. Phys.* **1994**, *101*, 7211−7220.
(36) Hunter, R. J. *Foundations of Colloid Science*; Oxford University Press: New York, 1989.
(37) Sein, A.; Engberts, J. B. F. N. *Langmuir* **1995**, *11*, 455−465.

MA980918Z